

Preparation and Activation of Corn Straw-Based Carbon and Its Application in Supercapacitors

Gaofeng Shi*, Hongquan Zhang, Yucan Dong*, Qi Zhang, Zhao Wang, Xia Jiang, Yawen Hu, Fenfang Luo, Xin li, Guoying Wang

School of Petrochemical Engineering, Lanzhou University of Technology, NO.287, Langongping Road, Lanzhou, Gansu, China

*E-mail: 923028088@qq.com

Received: 6 April 2019 / Accepted: 25 May 2019 / Published: 30 June 2019

The corn-staw is made into a biomass porous carbon material using three different activation methods. The porous carbon produced using KOH as the activator shows the best electrochemical performance compared to carbons produced by other methods. When the ratio of KOH to raw material is 2:1 and the activation temperature is 800 °C, the specific surface area of the obtained carbon material is 1067.11 m²·g⁻¹, and the capacitance reaches 239 F·g⁻¹ at a current density of 1 A·g⁻¹. In addition, the capacitance was maintained at 97.12% after 5000 charge and discharge cycles at a current density of 1 A·g⁻¹ in a 6 M KOH aqueous electrolyte. The conversion of corn-staw into green porous carbon materials not only enables them to be used at high values, but also solves the problem of pollution caused by the treatment of biomass waste.

Keywords: activated carbon; various activation methods; electrode materials; capacitive performance

1. INTRODUCTION

Among various energy storage devices, supercapacitors can safely provide high power and fast charge/discharge, are environmentally friendly, have extremely long cycle life, and are flexible in operation and have attracted increasing attention from researchers worldwide. It is a type of energy storage device based on high-speed storage electrostatic or Faraday electrochemical processes. In a supercapacitor, the charge is mainly stored at the electrode-electrolyte interface of the active material. Therefore, the electrode material is the main factor determining the performance of supercapacitors. There are many kinds of electrode materials, which can be divided into carbon electrode materials, metal oxide electrode materials, conductive polymer electrode materials and composite electrode materials according to the composition of electrode materials [1]. Carbon electrode materials are most likely to be

industrially produced due to their relatively low price. Porous carbon materials (such as activated carbon, activated carbon fibres, carbon nanotubes, and template carbon) have stable chemical properties, developed pore structure, large specific surface area and no toxicity and are thus ideal materials for preparing electric double layer supercapacitor electrodes [2-6].

With the environmental pollution becoming increasingly serious and the non-renewable energy being depleted, developing renewable energy technologies has never been more imperative. Biomass waste, including but not limited to waste straw, animal waste, forestry waste, is rich in carbon, and it not only has a large amount of natural pore structure inside, but also contains elements such as nitrogen, achieve surface and internal in-situ doping of the carbon material, which all add to the capacitive performance of the carbon material. According to reports, the carbon content of corn stover is 42.82%, the oxygen content 38.35%, and the nitrogen content 1.30% [7]. The conversion of corn stalks into green carbon electrode materials, on the one hand, enables them to be used at high values, and on the other hand solves the problem of pollution caused by the treatment of biomass waste.

The carbon electrode material of the supercapacitors mainly uses an electric double layer to store energy at the electrode/electrolyte interface. Therefore, the specific surface area and pore size distribution of the material are the most important factors affecting their electrochemical performance. An appropriate pore size distribution is beneficial for reducing the diffusion resistance of the ions in the pore structure, thereby increasing the charge and discharge rates [8]. Increasing the specific surface area of carbon electrode materials for supercapacitors and establishing a reasonable distribution of pore structure has always been the focus of reserach. The activation methods of carbon electrode materials are mainly classified into physical activation methods and chemical activation methods. Physical activation uses oxidizing gases such as water vapour, carbon dioxide and supercritical water to open the pores that are originally blocked inside the carbon material, further reopening and generating pores to form a new pore structure [9,10]. Using KOH, NaOH, H₃PO₄ and transition metal salts (such as zinc salt, iron salts, nickel salts, cobalt salts) as activators [11-15], activated carbon materials with a developed pore size and a high specific surface area can be obtained by adding an activator in a certain proportion during the carbonization of the precursor.

In this paper, we use corn stalk as the raw material and potassium hydroxide as the activator in the carbonization process. The effects of the addition amount of KOH activator and carbonization temperature on the microstructure and electrochemical properties of biomass-based porous carbon materials were studied, and the optimal activation conditions and parameters were screened. At the same time, we used the Kumaresian method [16] and modified Hummers method [17] to make two other corn-straw-based porous carbon materials. The electrochemical properties of the porous carbon produced by the three methods were compared comprehensively, and the best method for preparing corn stover-based porous carbon was determined.

2. EXPERIMENTAL

2.1 Major instruments

A TL1200 tube furnace (Nanjing Boyuntong Instrument Technology Co., Ltd., Nanjing); An XMTD-8222 vacuum drying oven (Shanghai Jinghong Experimental Equipment Co., Ltd., Shanghai);

A Nexus 670 fourier transform infrared spectrometer (American Thermo Nicolet Corporation); A D/max-2400 x-ray diffractometer (Japan Rigaku Corporation); An ASAP 2020 specific surface area meter (Mike Instruments); A JSM-6701M cold field emission scanning electron microscope (Japan Electron Optics); And a CHI660E electrochemical Workstation (Shanghai Chenhua Instrument Co., Ltd., Shanghai) were used.

2.2 Experimental methods and processes

2.2.1 Preparation of Biochar by the Sulphuric Acid/Hydrogen Dioxide Method

The received corn straw powder was washed twice with distilled water to remove mud and impurities and was dried in a blast dryer at 80 °C for 24 h. Corn straw powder (30.0 g) was weighed in a 500 ml beaker with an electronic balance, and concentrated sulphuric acid (150 ml) was slowly added to carbonize, greatly expanding the corn stalk and releasing gas and a large amount of heat. After the temperature was lowered to room temperature, the mixture was stirred with a glass rod after carbonization. The corn stalks returned to their original volume. Next, 30% hydrogen peroxide (50 ml) was weighed and slowly added to the corn stalks, which were carbonized by sulphuric acid. During the period, a large amount of heat was released and the solution boiled many times. After cooling to room temperature, a large amount of distilled water was added and washed repeatedly with suction until the pH was close to 7. The resulting black powder was then dried overnight in a forced air oven at 120 °C to remove the moisture and was ground to a fine powder and stored. The resulting biomass charcoal was named CS-SHAC.

2.2.2 Preparation of Activated Carbon by Mixed Salt Method

The received corn straw powder was washed twice with distilled water to remove mud and impurities and was dried in a blast dryer at 80 °C for 24 h. The corn straw powder was carbonized in a muffle furnace at 300 °C for 2 h with a rate of temperature increase and decrease of 2 °C·min⁻¹. The temperature was lowered to room temperature, and then the precursor carbon was pulverized into a fine powder by a mortar and collected for further activation. Sodium chloride (NaCl) and potassium chloride (KCl) salts (molten salts) were mixed in a ratio of 1:1, and the molten salt was used as the solvent and activator. The precursor carbon (10 g) was mixed with the activator (10 g), distilled water was added, and the mixture was stirred at 70 °C in a stirrer until the water was evaporated. Then, it was dried in a blower box at 120 °C for 24 h. After drying, the carbon was activated at the optimal temperature of 900 °C for 2 h [18] at a nitrogen flow rate of 80 cm³·min⁻¹, the heating rate was 2 °C·min⁻¹, and the cooling rate was 5 °C·min⁻¹. Then, the mixture was treated with an excess of dilute hydrochloric acid and washed repeatedly with distilled water until all of the chloride ions were discharged. It was then dried overnight in a forced air oven at 120 °C to remove the moisture, ground to a fine powder, and packaged for later use. The obtained activated carbon was named CS-MSAC.

2.2.3 Preparation of activated carbon by KOH method

The received corn straw powder was washed twice with distilled water to remove mud and impurities and was dried in a blast dryer at 80 °C for 24 h. The corn straw powder (10 g) was mixed with the KOH (5 g, 10 g, and 20 g) ground in a mortar until thoroughly mixed. The carbon was activated at the optimal temperature of 800 °C for 2 h, the rate of temperature increase was 2 °C·min⁻¹, the rate of temperature drop was 5 °C·min⁻¹, then treated with an excess of dilute hydrochloric acid, and washed repeatedly with distilled water until neutral. The resulting black powder was then dried overnight in a forced air oven at 120 °C to remove the moisture and was ground to a fine powder and stored. The obtained activated carbons were named CS-AKAC801, CS-AKAC802 and CS-AKAC803, respectively. The effects of different activator ratios on the properties of carbon materials were examined, and the optimum amount of activator was selected. Then, under the condition of optimal activator addition, the carbonization is activated at the optimal temperature of 700 °C, 900 °C for 2 h the heating rate was 2 °C·min⁻¹, the cooling rate was 5 °C·min⁻¹, and then treated with an excess of dilute hydrochloric acid, Wash repeatedly with distilled water until neutral. It was then dried overnight in a forced air oven at 120 °C to remove the moisture, ground to a fine powder, and packaged for later use. The effects of different activation temperatures on the properties of carbon materials were examined and named as CS-AKAC700 and CS-AKAC900, respectively, and the optimal activation temperature was screened.

3. RESULT AND DISCUSSION

3.1 Effect of KOH Activation Process Parameters on Capacitance Performance

Corn straw-based activated carbon, acetylene black, conductive graphite and polytetrafluoroethylene dispersion (60% by mass) were added to the mortar in a mass ratio of 8: 0.75: 0.75: 0.5 and mixed thoroughly into a paste [19]. The paste was evenly spread on 2 cm×1 cm of foamed nickel in the application area of 1 cm×1 cm and was dried in a vacuum drying oven for 8 h and then pressed into an electrode sheet under a pressure of 6 MPa. Due to a small loss of activated carbon during the smear and tableting process, the mass of the nickel piece before and after coating was weighed, and the mass of the effective activated carbon supported on the nickel piece was calculated according to the ratio. The biomass-based activated carbon electrode sheet was used as the working electrode, a saturated calomel electrode (SCE) was used as the reference electrode, and a platinum plate electrode was used as the counter electrode, and a three-electrode system was constructed using 6 M KOH solution as the electrolyte [20]. Electrochemical performance tests including the cyclic voltammetry (CV) test and the constant current charge and discharge (GCD) test were carried out in the potential range from -1.0 to 0 V. The optimum process parameters of the KOH-activated corn straw were determined.

As shown in Fig. 1, the corn straw and KOH were thoroughly mixed in a ratio of 2:1, 1:1, 1:2, and then carbonized at the optimal temperature of 800 °C for 2 h under nitrogen protection conditions, and the activated carbon materials CS-AKAC801, CS-AKAC802 and CS-AKAC803 were prepared. The constant current charge and discharge images of these carbon materials show obvious isosceles triangle shapes, and the cyclic voltammetry (CV) curves are all rectangular-like, which indicates that

these materials have typical electric double layer capacitance characteristics. Calculate the specific capacitance formula [21]:

$$C_m = \frac{I\Delta t}{m\Delta V} \quad (1)$$

Note: C_m is the carbon material specific capacitance value, I is the discharge current, Δt is the discharge time, ΔV is the scan voltage window, and m is the electrode active material mass.

In the following figures, Fig.1 (A) is the constant current charge and discharge (GCD) diagram of carbon material at $1 \text{ A}\cdot\text{g}^{-1}$ current density. According to formula 1, the specific capacitances of the corn straw-based activated carbon materials CS-AKAC801, CS-AKAC802 and CS-AKAC803 were calculated to be $137.5 \text{ F}\cdot\text{g}^{-1}$, $159 \text{ F}\cdot\text{g}^{-1}$ and $239 \text{ F}\cdot\text{g}^{-1}$, respectively. CS-AKAC803 has the highest specific capacitance, which is consistent with the conclusions obtained for the carbon materials from cyclic voltammograms (Fig. 1D) at $20 \text{ mV}\cdot\text{s}^{-1}$. As the amount of activator KOH added increases, the specific capacitance of the material tends to increase, because the carbon material creates more pores, increasing the specific surface area of the material. At the same time, according to the mechanism of KOH activated carbon material, KOH makes carbon to leave in the form of CO_2 , reducing the final yield, the yields of CS-AKAC801, CS-AKAC802 and CS-AKAC803 are 27%, 25% and 20%, respectively. When the mass ratio of KOH as the activator to corn stalk reaches 3:1, the carbon leaves almost all in the form of CO_2 , and the yield drops to 4.1%, which loses the practical application value. In summary, the best mass ratio of KOH as an activator to corn straw is 2:1.

When KOH was used as the activator, CS-AKAC700, CS-AKAC800 and CS-AKAC900 were obtained at activation temperatures of $700 \text{ }^\circ\text{C}$, $800 \text{ }^\circ\text{C}$ and $900 \text{ }^\circ\text{C}$, respectively, under optimal conditions. Fig. 1C shows a graph of the constant current charge and discharge (GCD) of the carbon materials at the current density of $1 \text{ A}\cdot\text{g}^{-1}$. According to the formula, the GCD values of corn straw-based activated carbon materials CS-AKAC700, CS-AKAC800, and CS-AKAC900 were $148 \text{ F}\cdot\text{g}^{-1}$, $217 \text{ F}\cdot\text{g}^{-1}$ and $239 \text{ F}\cdot\text{g}^{-1}$, respectively. This is consistent with the conclusions obtained for the carbon materials from cyclic voltammograms (Fig. 1D) at $20 \text{ mV}\cdot\text{s}^{-1}$. When the carbonization temperature was $700 \text{ }^\circ\text{C}$, on the one hand, the K_2CO_3 produced during the activation process was not further decomposed into K_2O and CO_2 [22], the CO_2 generated by the decomposition does not carry out a further activation of the carbon material, and the specific surface area is low. On the other hand, the degree of graphitization is not as good as that of the carbon materials obtained at $800 \text{ }^\circ\text{C}$ and $900 \text{ }^\circ\text{C}$, which means that the conductivity is lowered, the internal resistance is increased, and the capacitance performance is reduced. When the carbonization temperature is $900 \text{ }^\circ\text{C}$, the corn straw is not pre-oxidized and stabilized. The temperature may be too high, leading to the collapse of the original plant carbon layer during the graphitization process, which increases the internal resistance, resulting in a slight decrease in capacitance performance compared to the carbon materials prepared at $800 \text{ }^\circ\text{C}$. In summary, the optimal carbonation activation temperature for the use of KOH as an activator is $800 \text{ }^\circ\text{C}$.

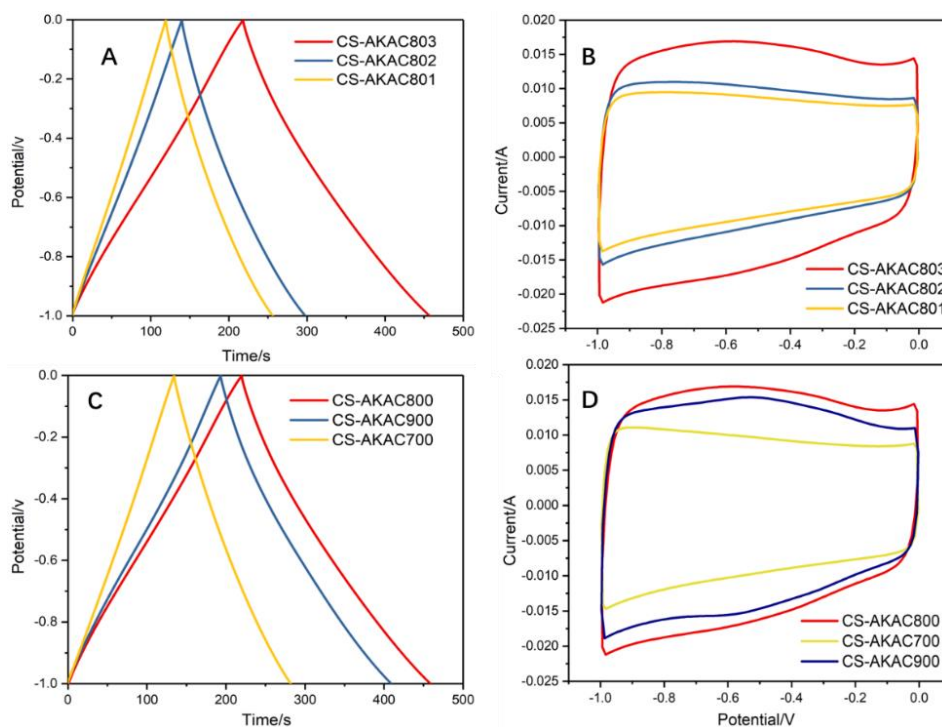


Figure 1. Electrochemical performance of a corn-staw based activated carbon electrode in a three-electrode system. A, B: CV curve of different activator addition amount at 800 °C ($20 \text{ mV}\cdot\text{s}^{-1}$) and GCD curve ($1 \text{ A}\cdot\text{g}^{-1}$); C, D: CV curve ($20 \text{ mV}\cdot\text{s}^{-1}$) and GCD ($1 \text{ A}\cdot\text{g}^{-1}$) curve of activated carbon of corn-staw prepared at different temperatures

3.2 Structural characterization of three different carbon materials

3.2.1 Morphological characteristics of three kinds of activated carbon

Figs. 2(A) and (D) show the SEM images of corn straw-based carbon materials CS-SHAC and ACs, and it is observed that these materials have no obvious pore structure on the surface and exhibit an overall carbon block structure. Fig. 2(B) shows an image of the activated carbon prepared using a mass ratio of 1:1 sodium chloride (NaCl) and potassium chloride (KCl) molten salt as the activator, and a porous block structure and a layered structure with a perforated sheet are observed. Due to the erosion of the molten salt at high temperatures, and the intercalation of metal cations as a template to ream, both bulk and sheet structure appear. The sheet structure has pores with a uniform pore diameter, and the block structure has different inwardly extending pore structures. This shows that this activation method can increase the specific surface area of the activated carbon material, which is beneficial for increasing the capacitance performance of the material. Fig. 2(C) shows an image of an activated carbon CS-AKAC803 fabricated using KOH as the activator. A large number of interconnected pores appear on the block structure, and KOH has a strong etching effect on the carbon material. Activated carbon prepared by the activation of molten salt and KOH with abundant macropores ($>50 \text{ nm}$) provides electrolyte storage, and mesopores ($2 \text{ nm}-50 \text{ nm}$) can provide a fast channel for ion transport, while micropores ($<2 \text{ nm}$) provide a sufficient number of active sites.

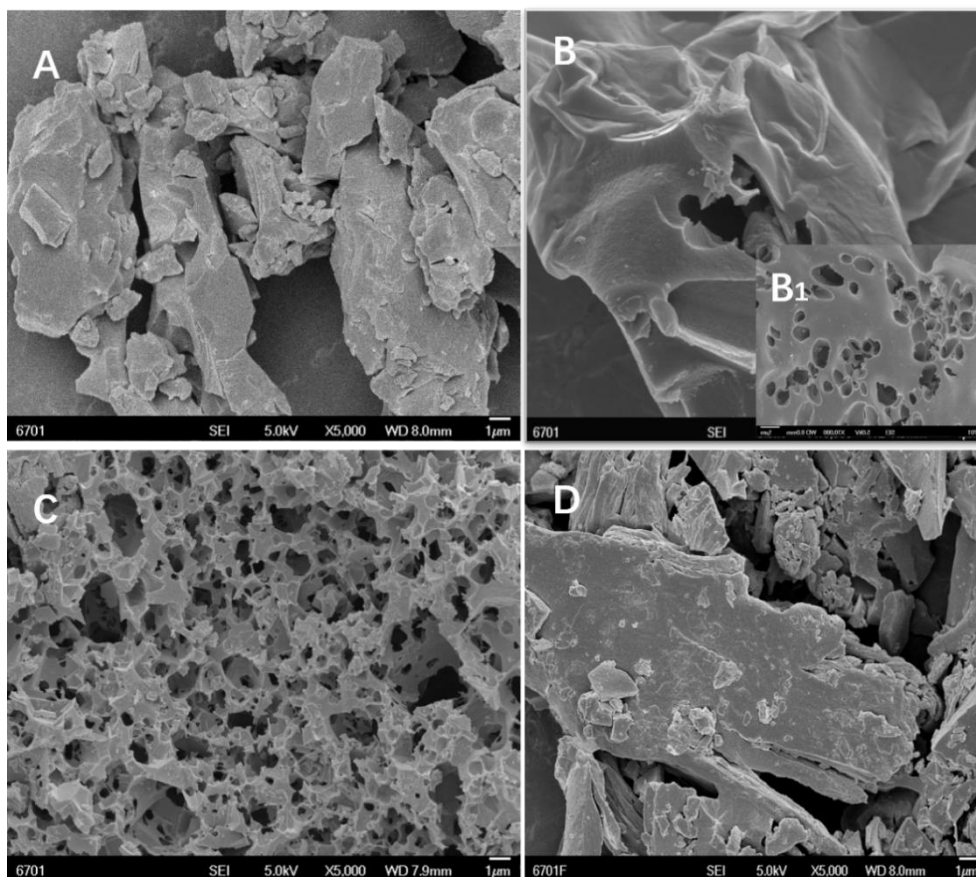


Figure 2. Scanning electron microscopy image of activated carbons prepared by different activation methods

3.2.2 Infrared spectra of three kinds of activated carbon

The chemical structure of the surface of three carbon materials was analysed by Fourier transform infrared spectroscopy (FTIR) using a Nexus 670 instrument in the scanning range of 400-4000 cm^{-1} [23]. As seen in Fig. 3, the absorption peak of the directly carbonized corn straw charcoal is relatively weak, indicating that there are fewer functional groups on the surface of the material. The characteristic peaks of the corn straw-based carbon materials CS-MSAC, CS-AKAC803, CS-SHAC at 1228 cm^{-1} , 1587 cm^{-1} and 3409 cm^{-1} obtained by molten salt activation, KOH activation, sulphuric acid and hydrogen peroxide carbonization were significantly enhanced. These peaks are respectively attributed to the stretching vibrations of the -CO, -C=C and -OH bonds on the surface of the activated carbon material. The peaks of the three carbon materials at 2854 cm^{-1} and 2923 cm^{-1} are due to the antisymmetric and symmetric stretching vibration of -C-H. The carbon material obtained by the carbonization of sulphuric acid and hydrogen peroxide has the largest peak value due to the strong oxidation of hydrogen peroxide under acidic conditions, which increases the oxygen-containing functional groups on the surface of the material [24]. The molten salt and KOH also increase the oxygen-containing groups on the surface of the corn straw during carbonization. According to the peak height of the infrared spectrum, the activated carbon material prepared by the activation of KOH has more functional groups than the carbon material prepared by the activation of the molten salt. The functional groups on the surface of these materials

increase the wettability of the material to the electrolyte, increase the effective specific surface area, and improve the capacitive properties of the carbon material.

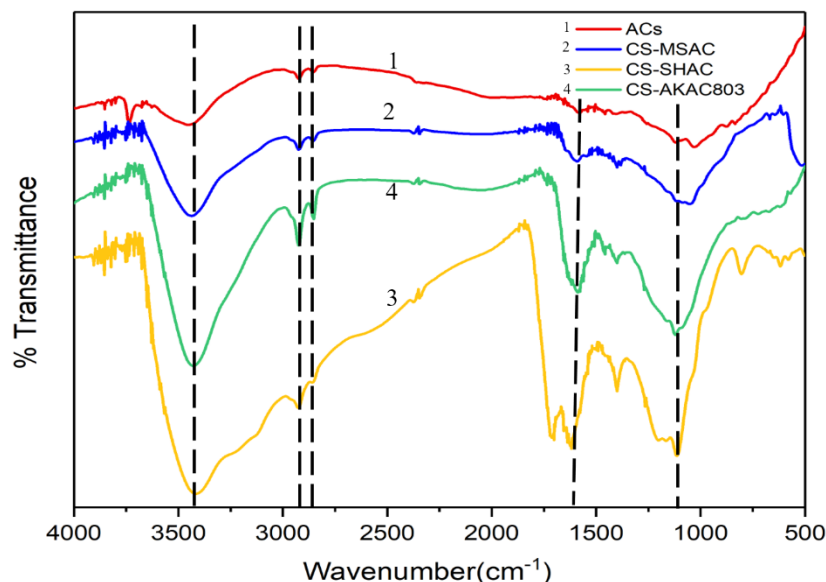


Figure 3. Infrared spectra of activated carbon prepared by different activation methods

3.2.3 XRD and Raman analysis of three activated carbons

To further examine the crystal structure of all samples, we used a D/max-2400C X-ray diffractometer (XRD) to characterize the three carbon materials. The diffraction source was Cu/K- α 1, and the scanning range was 5-80°. We performed XRD and Raman spectroscopy characterizations of the samples, the results of which are shown in Figure 4. It is observed from (A) that each sample has two broad characteristic peaks at 22.5° and 43.7° that correspond to the (002) crystal plane and the amorphous carbon (100) crystal plane of the graphite layer, respectively [25], indicating that the prepared sample consists of amorphous carbon and disordered carbon. Fig. 3(B) shows the Raman spectrum of the prepared sample. Two characteristic peaks can be clearly observed in the figure, namely, the D peak at 1335 cm^{-1} and the G peak at 1600 cm^{-1} . The D peak represents the disordered structure of the carbon material, and the G peak represents the graphitized structure [26]. Generally, the intensity ratio of the D peak to the G peak (I_D/I_G) is used to reflect the degree of structural disorder and the degree of graphitization in the carbon material [27]. The I_D/I_G values of the prepared corn straw-based carbon materials CS-SHAC, ACs, CS-MSAC, and CS-AKAC803 were 0.82, 0.94, 0.95 and 0.99, respectively, showing that the degree of disorder is highest for the CS-AKAC803 sample because the KOH activation process destroys the original carbon layer structure of the bio-stalk, and a more porous structure appears, in agreement with the SEM image observation.

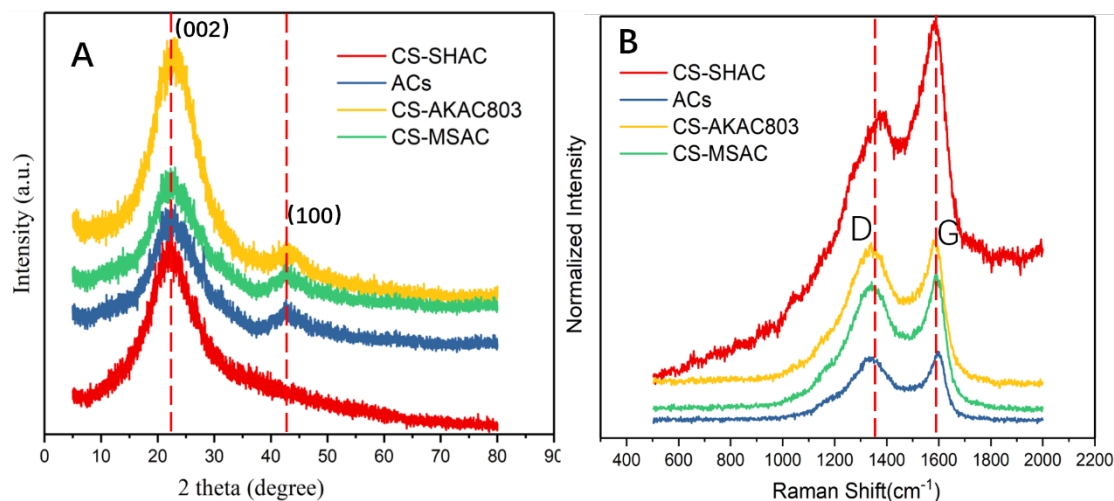


Figure 4. XRD and Raman spectra of carbon materials prepared using different activation methods

To study the microstructure of the material, we performed nitrogen adsorption-desorption characterization on all of the samples using an ASAP 2020 instrument at 77 K. The results are shown in Fig. 5(A). According to the classification of the Applied Chemistry Association (IUPAC), the nitrogen adsorption-desorption isotherm of porous carbon is a typical type IV isotherm, indicating that micropores (<2 nm) and mesopores (2 nm-50 nm) coexist. The CS-AKAC803 sample shows a sharp increase in adsorption volume at a lower relative pressure, indicating the presence of a large number of micropores. At higher relative pressures, the presence of mesopores causes a retention loop in the nitrogen adsorption-desorption curve that rises at the end of the curve. This trend indicates that a large pore structure is still retained. The results of the analysis and the characterization of the SEM images are similar to those of Su [28] who used KOH to activate a loofah to prepare long carbon. The nitrogen absorption and desorption curve of the CS-MSAC sample shows that the carbon material produced by the molten salt has a simultaneous microporous, mesoporous and macroporous structure due to the carbon etching type and the metal ion intercalation as the template remaining principle. However, it is deduced from the nitrogen adsorption amount that the pores of the material prepared by the KOH activation are more developed than the molten salt activation. The nitrogen absorption and desorption curve of the CS-SHAC sample shows that the sample obtained by this method has the least amount of nitrogen adsorption and the microporous and mesoporous structure compared with the carbon materials prepared by the other two methods. These structures may be derived from the pore structure of the material itself. The pore size distribution curve in Fig. 5(B) shows that all three materials contain microporous and mesoporous structures, which is consistent with the conclusion derived from Fig. 5(A).

As observed from an examination of the data presented in Table 1, the specific surface areas of the CS-AKAC803, CS-MSAC, and CS-SHAC samples were $1067.11 \text{ m}^2 \cdot \text{g}^{-1}$, $687.63 \text{ m}^2 \cdot \text{g}^{-1}$ and $391.36 \text{ m}^2 \cdot \text{g}^{-1}$, respectively. All three materials are microporous structures with the largest pore volume, indicating that the material structure prepared by the three methods is mainly a microporous structure. Among these, the KOH activation method is more developed than the pore structure of the materials obtained by the other two methods. The total pore volume of CS-AKAC803 is $0.64 \text{ cm}^3 \cdot \text{g}^{-1}$, and the micropore volume is $0.42 \text{ cm}^3 \cdot \text{g}^{-1}$, accounting for 65.6% of the total pore volume.

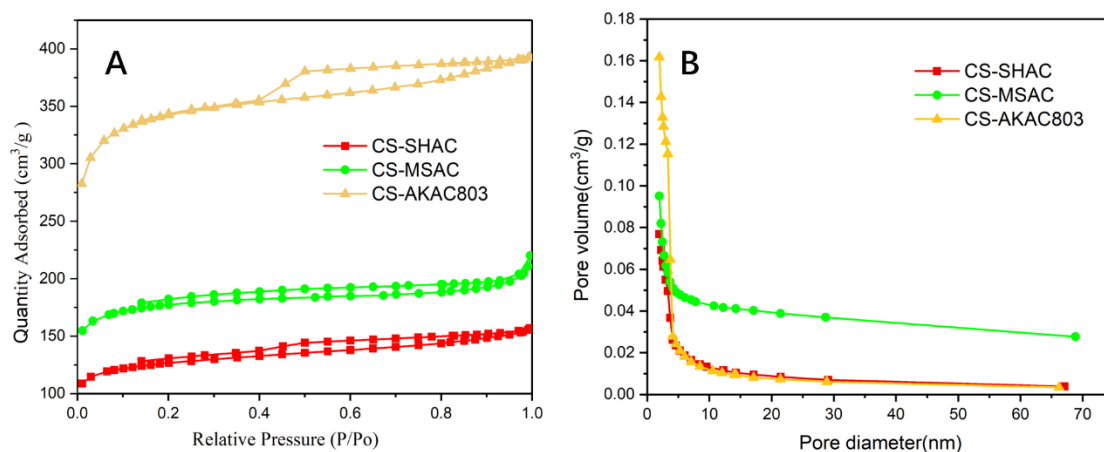


Figure 5. Nitrogen adsorption-desorption isotherms (a) and pore size distribution curves (b) for carbon materials obtained using different activation methods.

Table 1. Pore size distribution of porous carbon

Samples	S_{total} ($\text{m}^2 \cdot \text{g}^{-1}$)	V_{total} ($\text{cm}^3 \cdot \text{g}^{-1}$)	V_{micro} ($\text{cm}^3 \cdot \text{g}^{-1}$)	V_{meso} ($\text{cm}^3 \cdot \text{g}^{-1}$)
CS-SHAC	391.36	0.23	0.15	0.08
CS-MSAC	687.63	0.31	0.22	0.09
CS-AKAC803	1067.11	0.64	0.42	0.22

3.2.4 Characterization of the electrochemical properties of three different carbon materials

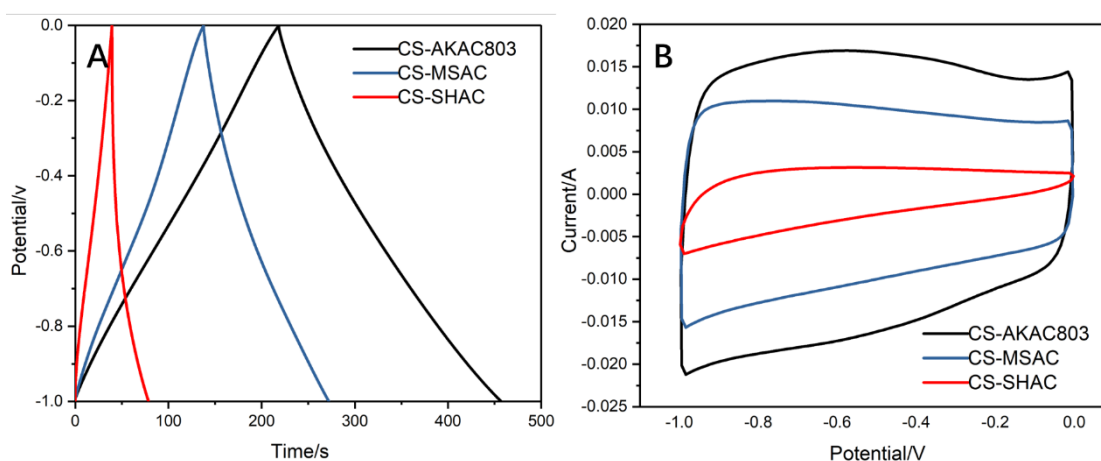
Using the CHI660E electrochemical workstation, with the platinum plate electrode as the counter electrode, the saturated calomel electrode as the reference electrode, and the activated carbon as the working electrode, the 6 M KOH aqueous solution is the electrolyte to form a three-electrode system. The cyclic voltammetry (CV) curve, constant current charge and discharge (GCD) curve and impedance (EIS) curve of three different material electrodes were tested in the voltage range of -1.0V -0V. The results are shown in Fig.6.

Figs. 6 (A) and 6(B) show the constant current charge and discharge (GCD) curves of three activated carbon materials at a current density of $1 \text{ A} \cdot \text{g}^{-1}$ and the cyclic voltammetry (CV) curves at a scan speed of $20 \text{ mV} \cdot \text{s}^{-1}$. The constant current charge-discharge curves of CS-AKAC803, CS-MSACCV and CS-SHAC have the shape of an isosceles triangle, and the cyclic voltammetry curves are all rectangular-like, indicating that these materials have typical electric double layer capacitance characteristics [29]. According to Equation 1, the specific capacitances of CS-AKAC803, CS-MSAC and CS-SHAC at the current density of $1 \text{ A} \cdot \text{g}^{-1}$ were $239 \text{ F} \cdot \text{g}^{-1}$, $135 \text{ F} \cdot \text{g}^{-1}$ and $54.15 \text{ F} \cdot \text{g}^{-1}$, respectively. The CV curve of CS-AKAC803 (Fig. B) has the largest area and the highest specific capacitance, consistent with the conclusions obtained from the constant current charge and discharge curve, showing that the activated carbon material obtained by KOH activation has the best capacitance performance.

Fig. 6(C) shows the constant current charge and discharge curves for CS-AKAC803 at different current densities. It is observed from the figure that the charging/discharging curves of the prepared

activated carbons are all isosceles triangles, indicating good electrical double layer capacitance performance. Fig. 6(C) shows the CV curves for CS-AKAC803 at different scan rates ranging from $20 \text{ mV}\cdot\text{s}^{-1}$ to $100 \text{ mV}\cdot\text{s}^{-1}$ in a potential window of $-1.0-0 \text{ V}$. Even at a high scan rate of $100 \text{ mV}\cdot\text{s}^{-1}$, the CV curve maintains a rectangular-like shape, indicating that the material has good fast charge/discharge capability and reversibility and good ion transport capability. As the sweep rate increases, the deviation of the CV curve from a rectangular shape increases because the current response increases with faster voltage changes, and the diffusion speed of the electrolyte in the electrode and the voltage change are not well balanced, the electrolyte ions cannot infiltrate inside the electrode active material and can only stay in the large holes of the surface or at the surface, resulting in a decrease in the effective surface area, an increase in internal resistance of the capacitor, and a decrease in capacitance performance [30]. Fig. 6(E) shows the rate performance curves of the three activated carbon materials. As the current density increases from $0.5 \text{ A}\cdot\text{g}^{-1}$ to $10 \text{ A}\cdot\text{g}^{-1}$, the specific capacitance of CS-AKAC803 decreases from $272 \text{ F}\cdot\text{g}^{-1}$ to $203.8 \text{ F}\cdot\text{g}^{-1}$. The rate is 74.93%, the specific capacitance of CS-MSAC is reduced from $150.8 \text{ F}\cdot\text{g}^{-1}$ to $108 \text{ F}\cdot\text{g}^{-1}$, and the capacitance retention rate is 72%; the specific capacitance of CS-SHAC is reduced from $54.15 \text{ F}\cdot\text{g}^{-1}$ to $9 \text{ F}\cdot\text{g}^{-1}$, and the capacitance retention rate is 16.62%.

In order to gain an in-depth understanding of the electrochemical properties of the three activated carbon materials, EIS measurements were performed and the results are shown in Fig.6 (F). In the high frequency region, the point intersecting the real axis reflects the internal resistance (R_s) of the electrode material, and the semicircle corresponds to the charge transfer resistance. The approximate vertical line in the low frequency region represents the diffusion resistance (W) of the electrolyte in the porous structure [31]. The curves of CS-AKAC803 and CS-MSAC have a small radius in the high frequency region and tend to be vertical in the low frequency region. The CS-SHAC curve has a large radius in the high frequency region and a small slope in the low frequency region. This means that the internal resistance and charge transfer resistance of the two electrode materials are small relative to CS-SHAC, and the diffusion resistance of the electrolyte is small, which increases the capacitance performance.



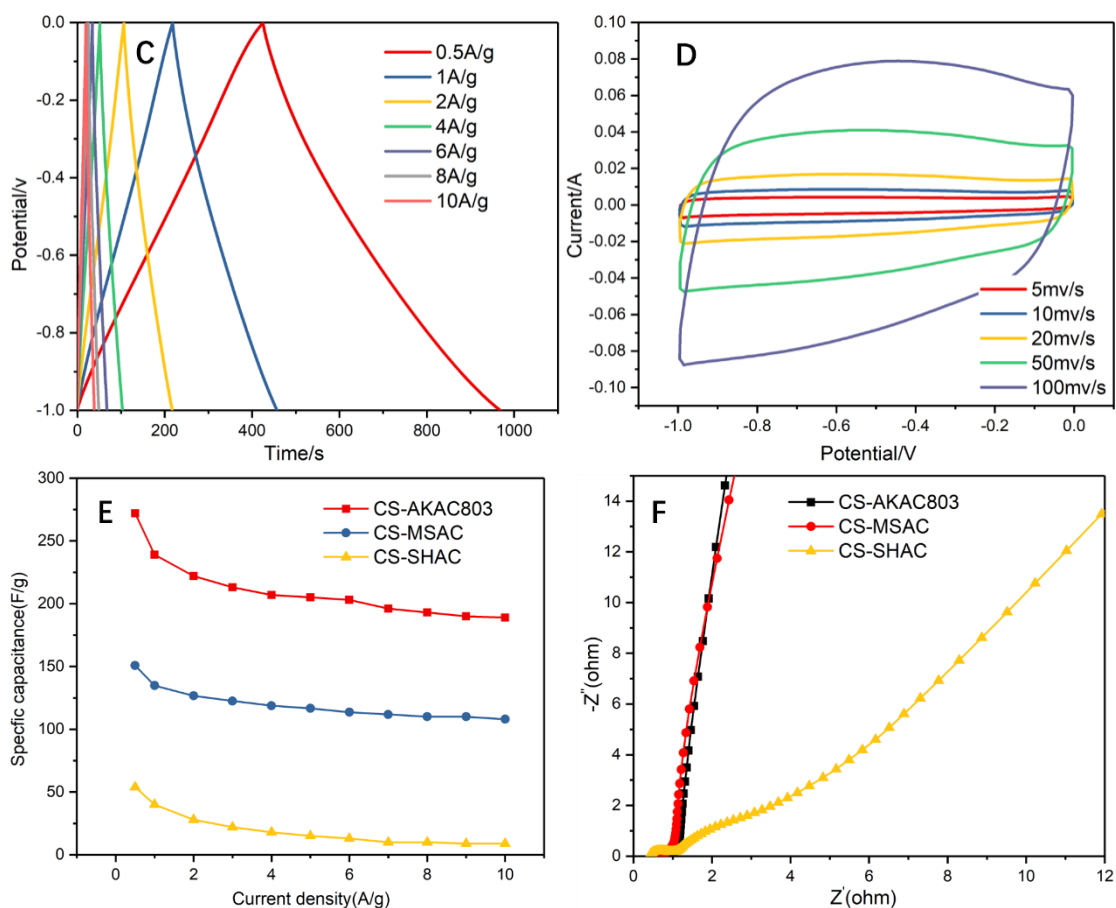


Figure 6. Characterization of electrochemical properties of the activated carbon prepared by different activation methods

Cyclic stability is an important parameter in the practical application of supercapacitor electrode materials. We tested the cycle stability of activated carbon materials with the results shown in Fig. 7. After 5,000 cycles of constant current charge and discharge at a current density of $1 \text{ A} \cdot \text{g}^{-1}$, CS-AKAC803 has a specific capacitance retention of 97.12% and CS-MSAC3 has a specific capacitance retention of 92.6%, showing excellent cycle stability. After CS-SHAC was cycled for 25 cycles, the active material of the electrode material began to decay strongly in the electrolytic cell, and the capacitance performance also drastically decreased. The above analysis shows that the excellent capacitance performance of CS-AKAC803 proves that it can be used as a supercapacitor electrode material.

To evaluate the superiority of the prepared electrode materials, Table 2 lists our results compared to previously published preparations of porous carbon by starch.

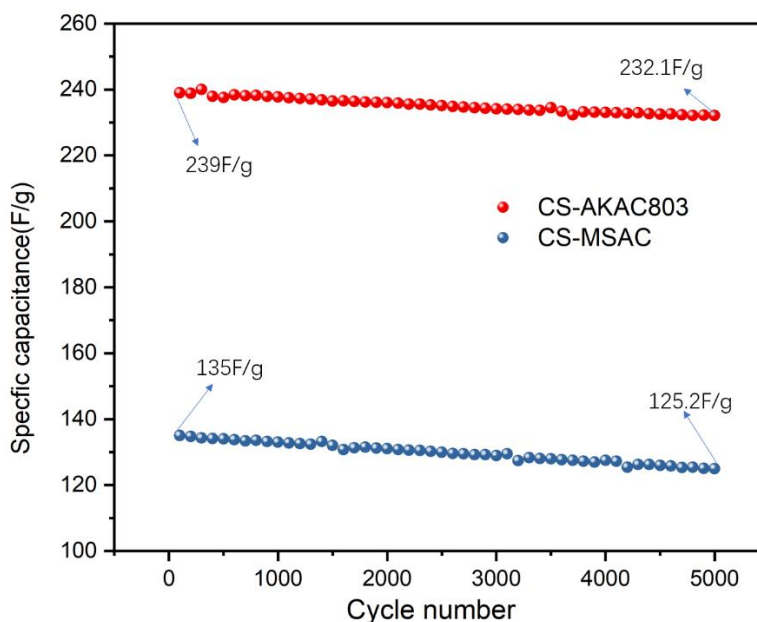


Figure 7. Cycle life diagram of the carbon materials circulating at 50,000 cycles at $1 \text{ A} \cdot \text{g}^{-1}$

Table 2. Comparison of electrochemical performance of porous carbon with other different material

Electrode materials	SBET ($\text{g} \cdot \text{m}^{-2}$)	Capacitance ($\text{F} \cdot \text{g}^{-1}$)	Current density ($\text{A} \cdot \text{g}^{-1}$)	Electrolyte	Ref.
Grapefruit skin	807.7	240	0.5	2 M KOH	[32]
Bagasse	1360	173.2	1	6 M KOH	[33]
Kapok tree shell	1260	169	1	6 M KOH	[16]
Corn Straw	1067.11	239	1	6 M KOH	This work

4. CONCLUSIONS

In this work, three kinds of biomass carbon electrode materials were prepared by using different methods for the treatment of corn straw. When KOH was used as the activator, the mass ratio of activator to corn straw was 2:1, and the activation temperature was $800 \text{ }^\circ\text{C}$. The prepared activated carbon electrode material has the best electrochemical performance. The KOH-activated corn straw-based activated carbon electrode material has a high specific surface area of $1067.11 \text{ m}^2 \cdot \text{g}^{-1}$, the specific capacitance reached $239 \text{ F} \cdot \text{g}^{-1}$ at $1 \text{ A} \cdot \text{g}^{-1}$ current density, and the specific capacitance retention rate was 97.12% after 5,000 cycles of constant current charge and discharge at the current density of $1 \text{ A} \cdot \text{g}^{-1}$. The waste corn stalk is converted into energy material by this activation method that not only improves the utilization rate of corn stalk but also solves the environmental pollution problem caused by burning straw, displaying excellent potential for future development.

ACKNOWLEDGEMENTS

This work was supported by the National Natural Science Foundation of China (21567015), the National Key Research and Development Program of China (2016YFC0202900), Lanzhou university of technology hongliu first-class discipline construction program and Lanzhou university of technology Hongliu Science Fund for Young Scholars (2018).

References

1. C. Zhong, Y. Deng, W. Hu, J. Qiao, L. Zhang and J. Zhang, *Chem. Soc. Rev.*, 44 (2015) 7484.
2. A.G. Pandolfo and A.F. Hollenkamp, *J. Power Sources*, 157 (2006) 11.
3. N. Bhattarai, Z. Li, D and M. Zhang, *Adv. Mater.*, 18 (2010) 1463.
4. G. Gryglewicz, J. Machnikowski, E. Lorenc-Grabowska, G. Lota and E. Frackowiak, *Electrochim. Acta.*, 50 (2005) 1197.
5. J. Yu, W. Lu and S. Pei, *Acs. Nano.*, 10 (2016) 5204.
6. A. Ameli, M. Nofar and C.B. Park, *Carbon*, 71 (2014) 206.
7. P. Wang, J. Chang and Q.Q. Yin, *Bioresour. Technol.*, 12 (2015) 165.
8. H. Shi, *Electrochim. Acta*, 41 (1996) 1633.
9. D.N. Futaba, K. Hata, T. Yamada, T. Hiraoka, Y. Hayamizu, Y. Kakudate, O. Tanaike, H. Hatori, M. Yumura and S. Iijima, *Nat. Mater.*, 5 (2006) 987.
10. Q.Y. Sun, T.Y. Jiang, G.Z. Zhao and J.Y. Shi, *Int. J. Electrochem. Sci.*, 14 (2019) 1.
11. S. Zhao, C.Y. Wang, M.M. Chen and Z.Q. Shi, *New Carbon Mater.*, 25 (2010) 43.
12. J.A. Yi, Y. Q and C. T. Wu, *J. Power Sources*, 351 (2017) 130.
13. D. Zeng, Y.P. Dou and M. Li, *J Mater Sci.*, 53 (2018) 8372.
14. Whittingham, M.S. *Chem. Rev.*, 104 (2004) 4271.
15. T. Brezesinski, J. Wang, S.H. Tolbert and B. Dunn, *Nat. Mater.*, 9 (2010) 146.
16. K. T. Kumar, G. S. Sundari, E. S. Kumar, A. Ashwini, M. Ramya, P. Varsha, R. Kalaivani, M. S. Andikkadu, V. Kumaran, R. Gnanamuthu, S. Zh. Karazhanov and S. Raghu. *Mater. Lett.*, 218 (2018) 181.
17. N.J. Song and C.L. Ma, *Int. J. Electrochem. Sci.*, 13 (2018) 452.
18. L. Zhou, X. J. Lin, T. Huang and A. S. Yu. *Electrochim. Acta*, 116 (2014) 210.
19. Z. Y. Lin, X. B. Yan, J. W. Lang, R. T. Wang and L. B. Kong. *J. Power Sources*, 279 (2015) 358.
20. L. Zhang, F. Zhang, X. Yang, K. Leng, Y. Huang and Y.S. Chen, *Small*, 9 (2013) 1342.
21. M. H. Yu, T. Zhai, X. H. Lu, X. J. Chen, S. L. Xie, W. Li, C. L. Liang, W. X. Zhao, L. P. Zhang and Y. X. Tong. *J. Power Sources*, 239 (2013) 64.
22. O. Y. Podyacheva, A. I. Stadnichenko, S. A. Yashnik, O. A. Stonkus, E. M. Slavinskaya, A. I. Boronin, A. V. Puzynin and Z. R. Ismagilov. *J. Catal.*, 35 (2014) 960.
23. R.T. Wang, P.Y. Wang, X.B. Yan, J.W. Lang, C. Peng, Q.J. Xue, *ACS Applied Mater. & Interfaces*, 4 (2012) 5800.
24. L. Yao, Q. Wu, P. X. Zhang, J. M. Zhang, D. R. Wang, Y. L. Li, X. Z. Ren, H. W. Mi, L. B. Deng and Z. J. Zheng. *Adv. Mater.*, 30 (2018) 170.
25. H. L. W, Z. W. X, A. Kohandehghan, Z. Li, K. Cui, X. H. Tan, T. J. Stephenson, C. K. Kingondu, C. M. B. Holt, B. C. Olsen, J. K. Tak, D. Harfield, A. O. Anyia and D. Mitlin. *Acs Nano*, 7 (2013) 5131.
26. X. L. Su, S. H. Li, S. Jiang, Z. K. Peng, X. X. Guan and X. C. Zheng. *Adv. Powder Technology*, 29 (2018) 2097.
27. L. J. Zhang, Y. Z. Jiang, L. W. Wang, C. Zhang and S. X. Liu. *Electrochim. Acta.*, 196 (2016) 189.
28. X. L. Su, J. R. Chen, G. P. Zheng, J. H. Yang, X. X. Guan, P. Liu and X. C. Zheng, *Applied Surface Science*, 436 (2018) 327.
29. Sabina P, Eyal Z and Yachin C. *Nano.*, 19 (2008) 603.
30. W. Li, F. Zhang, Y. Q. Dou and Z. X. Wu. *Adv. Energy Mater.*, 1 (2011) 382.

31. Jalili R, Morshed M and Ravandi S A H. *J. Appl. Polym. Sci.*, 101 (2010) 4350.
32. Z. Wang, Y. T. Tan, Y. L. Yang, X. N. Zhao, Y. Liu, L. Y. Nin, B. Tichnell, L. B. Kong, Z. Liu and F. Ran. *J. Power Sources*, 378 (2018) 499.
33. S. S. Gunasekaran, S. K. Elumalali, T. K. Kumaresan, R. Meganathan, A. Ashok, V. Pawar, K. Vediappan, G. Ramasamy, S. Zh. Karazhanov, K. Raman, R. S. Bose. *Mater. Lett.*, 218 (2018) 165.

© 2019 The Authors. Published by ESG (www.electrochemsci.org). This article is an open access article distributed under the terms and conditions of the Creative Commons Attribution license (<http://creativecommons.org/licenses/by/4.0/>).